WILEY
Biotechnology and Bioengineering

Engineering a thermostable fungal GH10 xylanase, importance of N-terminal amino acids

Journal:	*Biotechnology and Bioengineering*
Manuscript ID:	14-853.R1
Wiley - Manuscript type:	Article
Date Submitted by the Author:	n/a
Complete List of Authors:	Song, Letian; Institut national de la recherche scientifique, INRS-IAF Tsang, Adrian; Concordia University, Centre for Structural and Functional Genomics Sylvestre, Michel; Institut national de la recherche scientifique, INRS-IAF
Key Words:	Glycoside hydrolase, GH10, Directed evolution, Thermostability, Structure analysis, Biocatalysis

Engineering a thermostable fungal GH10 xylanase, importance of N-terminal amino acids

Letian Song[a], Adrian Tsang[b] and Michel Sylvestre*[a]

[a] *Institut National de la Recherche Scientifique, INRS-Institut Armand-Frappier, Laval, QC H7V 1B7, Canada*
[b] *Centre for Structural and Functional Genomics, Concordia University, 7141 Sherbrooke St. W., Montreal, QC H4B 1R6, Canada*

***Corresponding author:**

Michel Sylvestre, Institut National de la Recherche Scientifique, INRS-Institut Armand-Frappier, Laval, QC H7V 1B7, Canada, Phone: 450-687-5010; Fax: 450-686-5309, E-mail : michel.sylvestre@iaf.inrs.ca

Running Title~~head~~: Engineering a thermostable GH10 xylanase

Abstract

Xylanases are used in many industrial processes including pulp bleaching, baking, detergent and the hydrolysis of plant cell wall in biofuels production. In this work we have evolved a single domain GH10 xylanase, Xyn10A_ASPNG, from *Aspergillus niger* to improve its thermostability. We introduced a rational approach involving as the first step a computational analysis to guide the design of a ~~random~~ mutagenesis library in targeted regions which identified thermal important residues that were subsequently randomly mutagenized through rounds of iterative saturation mutagenesis (ISM). Focusinged on five ~~mutational positions~~residues, four rounds of ISM hadve generated a quintuple mutant 4S1 (R25W/V29A/I31L/L43F/T58I) which exhibited thermal inactivation half-life ($t_{1/2}$) at 60°C that was prolonged by 30 folds in comparison with wild-type enzyme. Whereas the wild-type enzyme retained 0.2% of its initial activity after a heat treatment of 10 min at 60°C and was completely inactivated after 2 min at 65°C, 4S1 mutant retained 30% of its initial activity after 15 min heating at 65°C. Furthermore, the mutant melting temperature (T_m) increased by 17.4°C compared to the wild type. Each of the five mutations in 4S1 was found to contribute to thermoresistance, but the dramatic improvement of enzyme thermoresistance of 4S1 was attributed to the synergistic effects of the five mutations. Comparison of biochemical data and model structure between 4S1 and the wild-type enzyme suggested that the N-terminal coil of the enzyme is important in stabilizing GH10 xylanases structure. Based on model structure analyses, we propose that enforced hydrophobic interactions within N-terminal elements and between N- and C-terminal ends are responsible for the improved thermostability of Xyn10A_ASPNG.

Key words: Glycoside hydrolase; GH10; directed evolution; thermostability; structure analysis; biocatalysis

Introduction

Endo-β-1,4-xylanases (EC 3.2.1.8) are glycosyl hydrolases (GH) commonly known as xylanases. They randomly attack and depolymerize the β-1,4-linkages between xylosyl units in the xylan backbone (Berrin and Juge 2008; Zimmermann 1991). Within the CAZy classification xylanases are found among GH families 5, 8, 43, and principally in GH10 and GH11 (Dumon et al. 2012; Henrissat and Bairoch 1996). Xylanases contribute significantly to the biodegradation of lignocellulosic biomass, not only because they breakdown inherent heteroxylans into short oligomers or even xylose, but also because they help to improve access to the other cross-linked components of plant cell wall (Kumar and Wyman 2009; Lynd et al. 2005; Somerville et al. 2004; Song et al. 2012; Watanabe 1989). As a result, xylanases facilitate the ~~releasing~~ release and/or depolymerization of~~zing~~ cellulose and lignin in the lignified plant cell wall. Due to these abilities, ~~in recent years~~ xylanases have been the focus of extensive investigations for their potential applications in the next generation of biorefinery (Shallom and Shoham 2003; Wyman 2007). Nevertheless, xylanases are currently utilized in the food, animal feed, detergent and paper industries (Collins et al. 2005; Kulkarni et al. 1999).

In the paper industry, the use of xylanases in the bleaching of Kraft pulp is an attractive practice. Here, xylanases disrupt the intimate contacts of the lignin-polysaccharide complex in the unbleached pulp, and thus improve the efficient extraction of residual lignin that is responsible for the brown color (Ragauskas et al. 1994; Roncero et al. 2005; Viikari et al. 1994). Compared to chlorine-mediated bleaching, xylanase treatment is highly specific~~,~~ and it is an environmental friendly process that circumvents many problems associated with chemical methods (Khonzue et al. 2011; Paice and Zhang 2005;

Viikari et al. 1994). Several studies have highlighted the high temperatures (> 50°C) applied in industrial bio-bleaching process (Buchert et al. 1994; Kulkarni et al. 1999; Viikari et al. 1994), and therefore it is necessary to develop suitable and robust enzymes bearing high pulp bleaching ability and thermostability. In a screen for pulp-bleaching enzymes, we identified a single domain GH10 xylanase of *Aspergillus niger* (gene ID NRRL3_08708; http://genome.fungalgenomics.ca/new_gene_model_pages/gene_model_page.php?nonav=yes&gmid=nrrl3_08708) that possesses strong pulp-bleaching activity (unpublished data). We designated this xylanase as Xyn10A_ASPNG (referred to as Xyn10A in this study) and it is identical to the translated sequence of *xynA* from *A. niger* CBS 513.88 genome sequence (GenBank: AM270045.1). However, Xyn10A is rapidly inactivated at high temperature which restricts its potential to handle industrial tasks. To improve the potential application of Xyn10A in pulp bleaching, we initially tried several rational designs to evolve the enzyme. By comparing structural differences between a hyper-thermostable xylanase 10B (TmxB) from *Thermotoga maritima* (PDB code: 1VBR) and a modeled Xyn10A, the residue Ala-267 of Xyn10A was replaced by Arg in an attempt to generate two additional side chain-mediated hydrogen bonds to stabilize two parallel strands. Likewise, another variant was created by deleting 11 N-terminal residues that have been postulated to be an unstable region, in accordance with the results reported by Liu et al. (2011) who had studied a similar xylanase. However, no improvement of thermostability was obtained from both rational engineering efforts. In contrast, our data revealed that the deletion of the N-terminal reduces wild-type thermostability (unpublished).

Unlike rational designs, DNA randomization via error-prone PCR (epPCR) does not require an extensive knowledge of protein structure (Arnold and Moore 1997). Indeed, such a method has been widely applied to improve xylanase thermostability (Miyazaki et al. 2006; Ruller et al. 2008; Stephens et al. 2007; Xie et al. 2006; You et al. 2010; Zhang et al. 2010), activity (Song et al. 2012) and alkaliphilicity (Chen et al. 2001; Inami et al. 2003; Stephens et al. 2009). However, approaches that randomize the whole target gene require the screening of large libraries of mutants. To reduce the size of the library to be handled, we introduced a rational approach involving as the first step a computational analysis to narrow the range of sequences for random mutagenesis. We expected the mutant library resulting from the epPCR mutagenesis to allow identification of thermal important residues for subsequent rounds of iterative saturation mutagenesis (ISM). The robustness of ISM has already been successfully tested on other enzymes and it has been shown to be a valuable approach to expand fitness of residual sequence space and find out the best additive and/or cooperative effects within mutations at different sites (Reetz and Carballeira 2007; Reetz et al. 2006; Wen et al. 2012; Wu et al. 2013). As described in this work, a semi-rational, directed evolution approach exploiting a combination of *in silico* assisted random mutagenesis via epPCR and ISM, coupled with a high-throughput screening protocol was successfully used to evolve thermoresistant xylanases. The structures of the wild-type and mutant enzymes were modeled and analyzed to shed insights into the structural features of Xyn10A that may impact on thermostability.

Materials and Methods

General

Escherichia coli C41(DE3) (Miroux and Walker 1996) and plasmid pET-20b (Novagen, Madison, WI) were used in this study. All chemicals and reagents, unless otherwise stated, were purchased either from Sigma-Aldrich (St Louis, MO, USA) or Fisher Scientific (Ottawa, Canada). Restriction enzymes, Phusion DNA polymerase, T4 DNA ligase and their corresponding buffers were purchased from New England Biolabs (Beverly, MA, USA). Oligonucleotide primers were synthesized by Alpha DNA (Montreal, Canada), and DNA was sequenced at the McGill University-Génome Québec Innovation Centre (Montreal, Canada). The 96-well microtiter plates for bacterial growth were purchased from Becton Dickinson Labware (Franklin Lakes, NJ, USA), and the other microtiter plates were from Corning Corp. (Corning, NY, USA).

Random Mutagenesis of Xyn10A N-Terminal by epPCR

Random mutagenesis ~~was carried out~~ by epPCR was conducted using GeneMorph® II random mutagenesis kit (Stratagene, La Jolla, CA, USA). The ~~template was the~~ DNA sequence encoding the mature protein of Xyn10A was used as template. It was constructed by ~~cleavage of~~removing the DNA segment, encoding the first 19 N-terminal amino acids, corresponding to the signal peptide as predicted by PredSi (http://www.predisi.de/predisi) ~~that involves, the first 19 N-terminal amino acids~~. The template DNA was cloned ~~at~~ into the *Nde*I / *Xho*I sites in the vector pET-20b, and the resulting recombinant protein is ~~recognized as~~considered the wild type in this study. In epPCR, only 260 nucleotide pairs at the 5'-end of the cloned *xyn10A* gene were

randomized. Briefly, 1.5 ng of template DNA~~,~~ and 125 ng each of forward (5'-TGTTTAACTTTAAGAAGGAGATATACATATGG-3') and reverse (5'-ACACGAGAGTATGTCCGCGG-3') primers were used in a 50 µL reaction mixture. PCR reaction was conducted as follows: 95°C for 2 min followed by 30 cycles of 95°C for 30 sec, 51°C for 30 sec and 72°C for 1 min, and finally 10 min extension at 72°C. The products were double-digested by *Nde*I and *Sac*II, and then ligated with similarly digested ~~template~~ vector DNA. The ligation mixture was transformed into *E. coli* C41(DE3) ~~through~~ by electroporation.

Saturation Mutagenesis

Saturation mutagenesis was accomplished using a Phusion DNA polymerase-mediated PCR reaction. Plasmids containing wild-type or mutant *xyn10A* genes were used as templates. All primers were phosphorylated at the 5'-end. Table 1 lists the sequences of degenerate primers and annealing temperatures used in each experiment. The PCR reaction mixture (50 µL) contained 10–50 ng of template DNA, 0.5 µM of primer pairs, 200 µM dNTPs and 1U of DNA polymerase. The amplification was ~~carried out~~performed as follow: 98°C for 30 sec, 25 cycles of 98°C for 10 sec, 30 sec at relevant annealing temperature and 72°C for 2.5 min, and 1 cycle at 72°C for 10 min. Then the PCR mixture was treated with *Dpn*I at 37°C for 1 hour to digest the template DNA. The final PCR amplified products were purified and used to transform *E. coli* C41(DE3) competent cells.

High-Throughput Screening of Mutant Libraries

Mutant libraries were created in *E. coli* C41(DE3). The microtiter plate-based cultivation and induction of mutant library individuals was performed according to a previously described method (Song et al. 2010). Recombinant *E. coli* cells were lysed by adding 40 µl of CelLytic B per well and incubating for 20 min at room temperature at 100 rpm. The cell lysates were then mixed with sodium acetate reaction buffer (50 mM, pH 5.5) to a final volume of 200 µL. Cell debris were removed by centrifugation (3,000 g, 10 min), and 40 µL of supernatant from each well were transferred into a new ~~PCR-bottom~~ microtiter plate and covered with a polypropylene lid. ~~The xylanase~~Heat inactivation ~~treatment~~ of enzyme activity was achieved by ~~heating~~ placing each microplate in a heating block (filled with water) at the desired temperatures and incubation times. Heat treatment at 58°C for 15 min was used to screen the random mutagenesis library. Treatment conditions of 60°C for 20 min, 65°C for 10 min and 70°C for 6 min were respectively employed to screen the different ISM libraries. The heat treatments were terminated by transferring the microplates to an ice bath. To measure residual activity of each clone, 40 µL of 1% of beechwood xylan dissolved in the reaction buffer were dispensed into each well and the reaction mixtures were incubated at 50°C for 10 min. The hydrolysis was stopped by adding 80 µL per well of 3,5-dinitrosalicylic acid (DNS) and heating at 95°C for 20 min (Miller 1959). Absorbance at 540 nm was measured ~~for quantitative analysis~~to determine enzyme activity.

Recombinant Expression and Affinity Purification

E. coli C41(DE3), harboring either wild-type or variant *Xyn10A* plasmids ~~construction~~, was grown at 37°C in Luria–Bertani (LB) medium (Sambrook and Russell 2001) containing 100 mg/L ampicillin. Isopropyl β-D-thiogalactopyranoside (IPTG) (0.4 mM) was added to the culture when OD_{600nm} reached 0.7–0.8, followed by incubation overnight at 20°C. Cells were then collected, sonicated, and the C-terminal His-tagged xylanase was purified by affinity chromatography on high-performance nickel-Sepharose (GE Healthcare) according to the manufacturer`s recommendations. Enzyme purity was assessed using SDS-PAGE ~~with~~ followed by Coomassie staining, and the concentration was determined by spectrophotometry at 280 nm. Enzyme theoretical extinction coefficient was computed using the ProtParam tool in the ExPASy server (Gasteiger 2005).

Enzyme Characterization

Xylanase specific activity was determined by monitoring hydrolysis against 0.5% beechwood xylan in sodium acetate buffer (50 mM, pH 5.5) using aforementioned DNS method. One activity unit (1 U) was defined as the amount of xylanase required to release 1 µmol of equivalent xylose per min (Paës and O'Donohue 2006). Thermoactivity assays were carried out by measuring specific activity of wild-type or mutant Xyn10A at temperatures ranging between 40°C and 70°C.

Half-life time ($t_{1/2}$) for enzyme thermal inactivation at 60°C was determined for the wild-type and all of ISM selected Xyn10A mutants. Thermal inactivation assays were performed by incubating the enzyme at 60°C. At regular time intervals, residual xylanase

activity was determined at 50°C; the data versus time were fitted, and the enzyme $t_{1/2}$ value was deduced as a time when the enzyme retained half of its initial activity. For mutant enzymes of 3S1 and 4S1, their $t_{1/2}$ values at 65°C and 70°C were similarly assayed.

Xylanase melting temperature was determined from circular dichroism spectra measured on a Jasco J-810 spectropolarimeter equipped with a Peltier heat controller (Hachioji, Japan). The xylanase solution was adjusted to 10 μM in 20 mM Tris H_2SO_4 buffer, pH 7.5, and placed in a 0.2 cm path-length cuvette. The heat-induced change of enzyme was recorded from 35°C to 80°C. The spectral data monitored at 220 nm versus temperature were fitted to compute enzyme T_m value using the Jasco spectroscopy software.

Kinetic parameters were determined at 50°C and 60°C for mutants 3S1 and 4S1, and at 50°C only for wild-type Xyn10A. The reactions were monitored using the DNS method at eight concentrations of beechwood xylan, from 0.2% to 1.5%. The initial velocities of the reactions were plotted against substrate concentrations, and k_{cat} and apparent K_m ($K_{m\ app}$) were calculated using SigmaPlot V10.0.

Homology Modeling, In Silico Prediction of Flexible Residues and Intramolecular Interactions

Homology modeling of wild-type and mutant 4S1 Xyn10A was accomplished using Swiss-model Workspace (Arnold et al. 2006). Structure modeling was automatically constructed using default parameters and *Penicillium simplicissimum* xylanase (PDB code: 1B31) (86% identity with Xyn10A protein sequence) as template. Potential

unstable residues of Xyn10A were predicted by PoPMusic 2.0 algorithm (http://babylone.ulb.ac.be/old_popmusic) (Dehouck et al. 2011). It is a tool to estimate the stability changes upon mutation for each residue of a given protein. Using modeled wild-type Xyn10A structure as input, the flexibility of each residue was estimated through an accumulation of folding free energy changes ($\Delta\Delta$G) from all 19 possible substitutions. For any given site, large absolute value of $\Delta\Delta$G means low stability. For both wild-type and 4S1 Xyn10A models, the interior hydrogen bonds, aromatic and hydrophobic interactions were predicted using the Protein Interaction Calculator (Tina et al. 2007) based on default setups. Figures were prepared using PyMOL software.

Results

Construction and Screening of Mutant Libraries

In this study, the mature *A. niger* Xyn10A, after the removal of the predicted secretory signal peptide of 19 N-terminal amino acid residues, is considered as the wild-type enzyme, and is numbered from Met-1 of the pre-protein. Therefore, the first residue of the recombinant protein is Glu-20. We used PoPMusic (Dehouck et al. 2011) ~~with the aim of recognizing~~to predict potential key regions that ~~may~~ might be crucial for enhancing Xyn10A thermostability. The feature of flexibility for each residue of ~~a~~ the modeled Xyn10A was evaluated from the computation of protein folding free energy changes (-$\Delta\Delta$G) resulting from all possible amino acid substitutions. The computed estimation indicated that the vast majority of Xyn10A flexible residues were located in the first and the last 1/3 parts of the protein sequence (data not shown). Considering the results were based on a model rather than real structure, we focused the mutagenesis on

the N-terminal portion that is rich in flexible residues. Therefore, the first 259 bases of the *xyn10A* gene, corresponding to the ~~initial~~ first 87 N-terminal amino acids of the recombinant protein, were randomized using epPCR mutagenesis. A moderate mutation rate (6.4 base substitutions per kb) was controlled to allow for about 80% of library clones to be real mutants. DNA sequence analysis revealed that the transition:transversion mutation ratio was 0.7, indicating the mutations were relatively unbiased.

~~The microplate high~~ High-throughput method was used to measure residual xylanase ~~residual~~ activity of library individuals following a heat treatment at 58°C for 15 min. Subsequent to this treatment, the wild-type enzyme retained 0.8±0.1% of its original activity. Figure 1 provides a representative example of the screening results. Among 96 observations in this mutant-containing plate, including three wild-type controls, 94 individuals were inactivated, showing less than 1% of the original activity. Nevertheless, two clones exhibiting high residual activities~~,~~ were visually distinguishable as they displayed red color in DNS-based assay.

Of the 8092 epPCR transformants screened, 27 clones were thermostable, corresponding to 21 variants because four single mutation variants (R1H03, R1H12, R1H15 and R1H18) were ~~repeatedly~~ selected more than once (Table 2). In addition, a silent mutation of C165T and multiple synonymous codons usage at residues Val-29 and Lys-34 ~~caused~~ meant that the 21 variants were translated into 17 chimeric amino acid sequences involving 11 single-, 5 double- and 1 triple-mutants. In total, amino acid substitutions involved thirteen residues, and several substitutions such as R25C, V29L, L43F, T58I and Q100L occurred in different variants.

The 21 variants were confirmed to have enhanced thermoresistance by submitting eight individual colonies of each to heat treatments at 58°C for 15 min, 60°C for 10 min and 65°C for 5 min. As shown in Table 2, the most thermostable enzymes were variants R1H08 (V29L-I31L), R1H17/18 (T58I), R1H01 (R25C-L43F) and R1H06/07 (V29L), which ~~have~~ had ~~maintained~~ retained ~~some~~ activity following a treatment of 5 min at 65°C. When heating at 58°C for 15 min, the level of residual activity of the top four variants were between 14 and 26-folds greater than that of the wild type. These results suggest that positions 25, 29, 31, 43, and 58~~, which were mutated in the top hits,~~ are potential thermal-important locations.

The five amino acid residues ~~chosen~~ identified from random mutagenesis were selected to initiate a stepwise ISM evolution~~ary approach~~. Because sites 29 and 31 were positioned closely, they were mutated simultaneously, thus facilitating the mutant library construction. In the first round of ISM, three single-sites and one double-site were individually randomized by saturation mutagenesis using wild-type DNA as template. To ensure all possible permutations would be covered in the screen, the appropriate degenerate codons were employed in library creation (Reetz and Carballeira 2007) and at least 300 clones were screened for each of the single-site randomized libraries and 1200 clones for the double-site randomized library. Compared to the random mutagenesis library, ISM libraries were subjected to harsher inactivation conditions. Table 3 summarizes the screening results. In the first round, no thermostable clone was found in the library saturated at position 43. The best hits arising from the other three libraries were 1S1 (R25W), 1S2 (V29A-I31L), and 1S3 (T58I) respectively, and their

thermoresistance were sorted as 1S2 > 1S3> 1S1 on the basis of the activity remaining after 20 min treatment of crude extract at 60°C.

According to the ISM theory (Reetz and Carballeira 2007), initial cycle of ISM ranks the significance of each mutated position for desired property, which helps to prioritize the order in subsequent combinational generations. Therefore in the second ISM round, the DNA template was the 1S2 gene and the saturation mutagenesis was carried out at the site of the next best hit (position 58). This was continued in subsequent third and fourth cycles on position 25 and 43 respectively. According to the screening assay results (not shown) the best triple, quadruple, and quintuple mutants were 2S1 (V29A/I31L/T58I), 3S1 (R25W/V29A/I31L/T58I) and 4S1 (R25W/V29A/I31L/L43F/T58I), respectively. This was confirmed when purified enzymes were used to determine thermal resistance as shown in Table 3. Mutants herein displayed a stepwise increased thermostability resulting from the assemblage of beneficial mutations. It is noteworthy that the best thermostable mutant 4S1 retained 8% of its initial activity after heating at 70°C for 6 min, representing a dramatic improvement from the wild type.

Biochemical Characterization of Xyn10A Mutant Enzymes

Enzyme thermal inactivation half-life ($t_{1/2}$) and protein melting temperature (T_m) were used as criteria for evaluating xylanase thermostability. Table 3 lists the 60°C $t_{1/2}$ and T_m values of the top hit from each ISM library. Figure 2A and 2B show the evolution of Xyn10A thermostability along with ISM process. At 60°C, the $t_{1/2}$ of the wild-type Xyn10A is 1.0 min. The first ISM generation variants have half-lives that are 1.6 to 2.8 times longer than that of the wild-type. Nevertheless, due to the combined effect of sets

of beneficial mutations, the 60°C $t_{1/2}$ values of variants 2S1 and 3S1 were dramatically prolonged in comparison to their parental ~~template~~ protein (Fig. 2A). The top two variants, 3S1 and 4S1, have similar 60°C $t_{1/2}$ values of 29.0 min and 30.0 min, respectively, which are 30 times longer than the wild type. However, they display slightly more differences in their $t_{1/2}$ values at 65°C and 70°C, which are respectively 8.0 and 2.2 min for 4S1 and 6.0 and 1.7 min for 3S1.

T_m measurement is considered a valid method to assess protein folding stability (Kumar et al. 2000). The T_m value of the wild-type Xyn10A is 51.4°C. Through the first round of ISM, the T_m values were elevated by 3.6°C, 5.8°C and 7.4°C for variants 1S1, 1S3 and 1S2 respectively (Fig. 2B), which were in accordance to their rankings in screening assays. The T_m result suggests that all of the explored mutations are beneficial to the folding of Xyn10A structure. ~~Matching 60°C $t_{1/2}$ values~~In addition, the combination of mutations led to further ~~increment~~ improvement ~~of~~ in T_m values. Compared to the wild type, increases of 12.4°C, 14.9°C and 17.4 °C have been achieved in the combinational variants 2S1, 3S1 and 4S1, respectively.

To probe the influence of enhanced thermostability on, catalytic properties, we determined the thermoactivity (Fig. 3) and steady-state kinetics (Table 4) of the wild-type and six ISM variants of Xyn10A ~~were determined using beechwood xylan as substrate~~. The optimal temperature (T_{opt}) of the wild-type enzyme was 45-50°C. At 50°C, all mutant enzymes displayed similar specific activities as the wild type, ~~that~~ they were in the range of 407.8 – 436.1 U mg^{-1} (Fig. 3). T_{opt} were determined to be 55°C for variant 1S1, 60°C for variants 1S2, 1S3, 2S1 and 3S1, and 65°C for 4S1. With respect to the enzyme activity at T_{opt} (i.e. maximum activity) as compared to the wild type, variant 1S1

led to a slight 4% increase, and the percentage increment in variants 1S3 and 1S2 were 36% and 62%, respectively. The maximum activities of combinational variants 2S1, 3S1 and 4S1 were similar (682.3 – 712.3 U mg^{-1}), which represented an improvement of approximately 1.73-fold compared to the wild type.

Steady-state kinetics of the wild type, 3S1 and 4S1 are summarized in Table 4. When measured at 50°C, neither k_{cat} nor $K_{m\ app}$ value differed significantly for the three enzymes. ~~and t~~The calculated $k_{cat}/K_{m\ app}$ constant was almost the same. This revealed that the mutations affecting thermostability did not influence enzyme catalysis or substrate binding. When monitoring kinetics at 60°C, Michaelis constant values of variants 3S1 and 4S1 were almost identical to those measured at 50°C~~, ; neverthelesshowever~~, their turnover rates were increased by 48% and 53% respectively. The increase turnover rates ~~at higher temperature is~~ can be attributed to the enzyme's ability to remain active at higher temperature and thus still follow the Arrhenius rate law at temperatures at which the wild-type enzyme is inactivated.

Discussion

Thermostability is a crucial property that enables enzymes to work at practical industrial processes. Moreover elevated catalysis temperature may reinforce the reaction kinetics (Rogers and Bommarius 2010). Among multiple protein engineering approaches, directed evolution is the most robust one to improve enzyme thermostability (Wang et al. 2012). To reduce the size of the library to be screened for beneficial variants, it is however necessary to create small but smart mutant libraries (Reetz and Carballeira 2007). In this work we utilized an *in silico* approach to guide the design of a random mutagenesis

library, and relied on an ISM approach to ~~probe~~ identify the ~~best~~ optimal combination of mutations at selected sites.

We chose PoPMuSiC as the predictive tool because of its ~~reasonable~~ accuracy, ~~friendly~~ easy to use~~r~~ interface, and importantly, unlike other often adopted approaches such as B-Fitter (Reetz and Carballeira 2007) and FoldX (Schymkowitz et al. 2005), it is attuned to model structures (Dehouck et al. 2011). The predictive reliability of PoPMuSiC program towards crystal structures has been demonstrated in recent studies, the experimental substitutions at about 50% of the predicted promising sites have led to improved stability (Cabrita et al. 2007; Silva et al. 2013; Zhang and Wu 2011). Although the structure of Xyn10A used for PoPMuSiC prediction was based on modeling, which would decrease predictive accuracy, we obtained positive results by focusing random mutagenesis on a region predicted to be rich in structural flexible residues (i.e. ~~initial~~ the first 87 N-terminal amino acids). ~~The~~ This approach has led to a relatively high screening efficiency where 21 thermoresistant variants were selected from 8092 clones. Of the 13 positions experimentally identified by random mutagenesis as important in thermostability, only two positions (33 and 34) were similarly favored by PoPMuSiC prediction, which illustrates the difficulties of rational engineering of enzymes by using statistic models.

~~Focused~~ Focusing on five mutational positions identified by random mutagenesis, four rounds of ISM have increased the 60°C $t_{1/2}$ and T_m of Xyn10A by 30-fold and 17.4°C, respectively. Moreover, the increased thermostability did not affect enzyme catalytic profiles, as activity and kinetics of the mutant enzymes were very similar to that of the wild type. Our results reflect two merits of the ISM approach: 1) randomization at selected positions reduces the size of the library that is needed to be tested to cover the

vast majority of theoretical substitutions; and 2) ISM makes it possible to obtain hits comprising sets of highly beneficial synergistic mutations. The evolutionary itinerary of discovering the best variant 4S1 (R25W/V29A/I31L/L43F/T58I) fully embodies this principle. Thermostability assays confirmed that each of 4S1 point mutations ~~were~~ was beneficial mutation~~s~~. Nevertheless, 60°C $t_{1/2}$ analysis (Fig. 2A) revealed that each single (R25W or T58I) or double (V29A/I31L) mutation~~s~~ only conferred limited ~~progress~~ improvement to the enzyme thermostability. The two big leaps in the evolutionary process occurred when mutant 1S2 (V29A/I31L) was evolved into 2S1 (V29A/I31L/T58I) and then into 3S1 (R25W/V29A/I31L/T58I). Therefore, the dramatic improvement in enzyme thermostability may be attributed to the synergistic effects of the newly generated mutations (T58I or R25W) and those from preceding ISM rounds.

To gain insights into how each individual mutation may affect thermostability, the tertiary structure of 4S1 was modeled (Fig. 4A) and it was compared to the wild-type Xyn10A model. Both models display a TIM-barrel fold that is ~~a~~ highly conserved ~~structure of~~among GH10 family proteins. However, in both cases the structural conformation of residues 19 to 25 is lacking because the template xylanase from *P. simplicissimum* does not have the corresponding sequence (Schmidt et al. 1998). ~~With the exception of information on position 25, o~~Of the four other mutated locations, only residue V29A is partially exposed which results in a small change in surface conformation between the wild- type and 4S1 models. Correspondingly, a comparison of pairs of mesophilic and thermophilic xylanases highlighted that minor sequence and structural modifications may give rise to significant thermostability differences (Collins et al. 2005). Structure analysis revealed that the other three substituted residues I31L,

L43F and T58I are completely buried inside the structure, and none of the mutation at these sites impacted on the number of hydrogen bonds. Nevertheless, the hydrophobic interactions with surrounding residues are markedly enhanced, especially at positions 43 and 58. Due to the I31L substitution ~~of I31L~~, a new N- and C-terminal contact is created between Leu-31 and Leu-327 (Fig. 4B). In addition, the L43F substitution may generate a new putative aromatic packing involving residues Phe-35 and Phe-43 that may reinforce interactions between N-terminal strand β1 and helix α0. The L43F mutation creates additional hydrophobicity towards a cluster of C-terminal aliphatic amino acids including two βα loop residues Leu-264 and Leu-309, and residue Val-278 at helix α7 (Fig. 4B). Furthermore, the replacement of Thr-58 side chain by the more hydrophobic side chain of Ile induces an increase in surrounding hydrophobicity: 1) interacting with adjacent residues Pro-59 and Ile-62 that closely packs helix α1 on which they are both located; and 2) possibly interacting through van der Waals forces with residues Val-295 and Tyr-314 at the long loop linking C-terminal strand β8 and helix α8 (Fig. 4B). The residues in hydrophobic clusters and their long range interactions have been demonstrated to be crucial for stabilizing the fold of TIM-barrel proteins (Gromiha et al. 2004; Selvaraj and Gromiha 1998), and improvement of hydrophobic packing has been suggested as one of the major structural determinants for enhancing the thermostability of thermophilic GH10 xylanases (Lo Leggio et al. 1999). Xie et al. (2006) have illustrated the effects of changing hydrophobicity on the thermostability of a GH10 xylanase from *Cellvibrio mixtus*. They showed that substitution of Ala-334 of *C. mixtus* by Val has elevated enzyme T_m value by 3.5°C because the bulkier side chain of Val fills a local hydrophobic cavity and makes more contacts with surrounding aromatic residues within the cavity

than the single methyl group of Ala. Although explanations based on *in silico* model are speculative, we propose that the stabilizing mutations in 4S1 along with a cluster of N- and C-termini hydrophobic amino acids ~~tend~~ increase protein interior hydrophobicity ~~along with a cluster of N- and C-termini hydrophobic amino acids~~. Plausibly, this change enforces hydrophobic packing at the N-terminal and/or contacts with C-terminal region.

GH10 family xylanases display a variable N-terminal end and the sequence of N-terminal part is less conserved than the core region (Bhardwaj et al. 2012). ~~Nevertheless, m~~Multiple sequence alignments indicate that beneficial residues Leu-31 and Phe-43 in mutant 4S1 are respectively moderately and highly conserved in fungal thermostable GH10 family xylanases (Fig. 5A). In contrast, the equivalent positions of Trp-25, Ala-29 and Ile-58 in 4S1 are much less conserved. Regarding residue Phe-43 in 4S1, Lo Leggio et al. (1999) has suggested a structural function for the phenylalanine located at the corresponding position in a ~~hyper~~thermo~~philic~~stable xylanase from *Thermoascus aurantiacus* (TAX). On the basis of structure comparison with ~~methophilic~~ mesophilic xylanases, the high thermostability of TAX was presumed to correlate with a cavity filed by residues Phe-18, Val-252, Ile-264 and Val-266 which are equivalent to Phe-43, Val-278, Ile-290 and Val-292 of 4S1 (Fig. 4B). Cavities increase exposed hydrophobic surface with the solvent, and the resulting unfavorable interactions negatively act on protein stability. Similarly, it is likely that mutation L43F leads to an efficient packing of a hydrophobic core that is important in stability for fungal GH10 xylanases.

In the study with GH10 xylanase from *Bacillus sp.*NG-27 (BSX), Bhardwaj et al. (2010) had ~~experimentally~~ provided experimental data showing interactions between N- and C-terminal portions of the protein ~~which~~ play an important role in protein stability. These

interactions were attributed to the Pi-stacking contacts within the Phe4-Trp6-Tyr343 cluster. The same aromatic cluster was found in two other homologous xylanases from *Bacillus firmus* (BFX) and *Bacillus halodurans* S7 (BHX). Intriguingly, sequence alignment and structure superposition revealed two equivalent positions in the Xyn10A mutant sequences which involve the N-terminus Trp-25 and a conserved C-terminal residue Tyr-314, (Fig. 5B). Therefore, we propose that mutation R25W benefits Xyn10A thermostability through the formation of a putative Pi-stacking that leads to close contacts between N- and C-termini.

In the N-terminal portion of Xyn10A, the first eleven amino acids are assembled into an unusual long coil in front of the initial helix α0. This N-terminal coil is flexible and spatially close to the C-terminal. Liu et al. (2011) reported that deletion of these N-terminal disordered residues decrease enzyme T_{opt} and T_m values of a similar GH10 xylanase but it significantly increases $t_{1/2}$ at 50°C. In our findings, the two beneficial modifications, R25W and V31A, show the importance of N-terminal coil in protein stability that is possibly attributed to the interactions with the C-terminal end, and for which comprehensive studies are needed. In this regard, Kamondi et al. (2008) found that interactions between the N- and C-terminal regions of the hyper-thermostable TmxB from *T. maritima* MSB8 contribute significantly to thermostability. We have superposed the modeled structures of Xyn10A and of mutant 4S1 to that of TmxB (not shown). Overall, the three structures superposed well except that the C-terminal α8 helix of Xyn10A is half the length of the corresponding helix of TmxB. In both Xyn10A and TmxB the N-terminal α0 helix runs parallel to the C-terminal α8 helix, but the longer α8 helix of TmxB allows for significantly more interactions between its C- and N-terminal

portions than in Xyn10A. Based on our observations and those on TmxB (Kamondi et al. 2008), we ~~thus~~ propose that engineering the N-terminal and C-terminal structures to strengthen their interactions is important in evolving thermostable GH10 family xylanases.

Acknowledgements

This work was supported by Genome Canada and Génome Québec.

References

Arnold FH, Moore JC. 1997. Optimizing industrial enzymes by directed evolution. Adv Biochem Eng Biotechnol 58:1-14.

Arnold K, Bordoli L, Kopp J, Schwede T. 2006. The SWISS-MODEL workspace: a web-based environment for protein structure homology modelling. Bioinformatics 22(2):195-201.

Berrin JG, Juge N. 2008. Factors affecting xylanase functionality in the degradation of arabinoxylans. Biotechnol Lett 30(7):1139-50.

Bhardwaj A, Leelavathi S, Mazumdar-Leighton S, Ghosh A, Ramakumar S, Reddy VS. 2010. The critical role of N- and C-terminal contact in protein stability and folding of a family 10 xylanase under extreme conditions. Plos One 5(6):12.

Bhardwaj A, Mahanta P, Ramakumar S, Ghosh A, Leelavathi S, Reddy VS. 2012. Emerging role of N- and C-terminal interactions in stabilizing (*beta*/*alpha*)8 fold with special emphasis on Family 10 xylanases. Comput Struct Biotechnol J 2:e201209014.

Buchert J, Suurnakki A, Carlsson G, Hausalo T, Laine JT, Strom G, Viikari L. 1994. Characterization of surface-properties of conventional kraft pulps by enzymatic peeling. Abstracts of Papers of the American Chemical Society 207:25.

Cabrita LD, Gilis D, Robertson AL, Dehouck Y, Rooman M, Bottomley SP. 2007. Enhancing the stability and solubility of TEV protease using in silico design. Protein Science 16(11):2360-7.

Chen YL, Tang TY, Cheng KJ. 2001. Directed evolution to produce an alkalophilic variant from a *Neocallimastix patriciarum* xylanase. Can J Microbiol 47(12):1088-94.

Collins T, Gerday C, Feller G. 2005. Xylanases, xylanase families and extremophilic xylanases. FEMS Microbiol Rev 29(1):3-23.

Dehouck Y, Kwasigroch J, Gilis D, Rooman M. 2011. PoPMuSiC 2.1: a web server for the estimation of protein stability changes upon mutation and sequence optimality. BMC Bioinformatics 12(1):151.

Dumon C, Song L, Bozonnet S, Fauré R, O'Donohue MJ. 2012. Progress and future prospects for pentose-specific biocatalysts in biorefining. Process Biochem 47(3):346-357.

Gasteiger E, Hoogland, C., Gattiker, A., Duvaud, S., Wilkins, M. R., Appel, R. D., Bairoch, A. 2005. Protein identification and analysis tools on the ExPASy server. In: Walker JM, editor. The Proteomics Protocols Handbook. Totowa, New Jersey Humana Press p571-607.

Gromiha MM, Pujadas G, Magyar C, Selvaraj S, Simon I. 2004. Locating the stabilizing residues in (α/β)8 barrel proteins based on hydrophobicity, long-range interactions, and sequence conservation. Proteins 55(2):316-329.

Henrissat B, Bairoch A. 1996. Updating the sequence-based classification of glycosyl hydrolases. Biochem J 316 (Pt 2):695-6.

Inami M, Morokuma C, Sugio A, Tamanoi H, Yatsunami R, Nakamura S. 2003. Directed evolution of xylanase J from alkaliphilic *Bacillus* sp. strain 41M-1: restore of alkaliphily of a mutant with an acidic pH optimum. Nucleic Acids Res Suppl(3):315-6.

Kamondi S, Szilagyi A, Barna L, Zavodszky P. 2008. Engineering the thermostability of a TIM-barrel enzyme by rational family shuffling. Biochem Biophys Res Comm 374(4):725-730.

Khonzue P, Laothanachareon T, Rattanaphan N, Tinnasulanon P, Apawasin S, Paemanee A, Ruanglek V, Tanapongpipat S, Champreda V, Eurwilaichitr L. 2011. Optimization of xylanase production from *Aspergillus niger* for biobleaching of *Eucalyptus* pulp. Biosci Biotech Bioch 75(6):1129-1134.

Kulkarni N, Shendye A, Rao M. 1999. Molecular and biotechnological aspects of xylanases. FEMS Microbiol Rev 23(4):411-56.

Kumar R, Wyman CE. 2009. Effect of xylanase supplementation of cellulase on digestion of corn stover solids prepared by leading pretreatment technologies. Bioresource Technol 100(18):4203-13.

Kumar S, Tsai CJ, Nussinov R. 2000. Factors enhancing protein thermostability. Protein Eng 13(3):179-91.

Liu L, Zhang G, Zhang Z, Wang S, Chen H. 2011. Terminal amino acids disturb xylanase thermostability and activity. J Biol Chem 286(52):44710-44715.

Lo Leggio L, Kalogiannis S, Bhat MK, Pickersgill RW. 1999. High resolution structure and sequence of *T. aurantiacus* xylanase I: implications for the evolution of thermostability in family 10 xylanases and enzymes with (*beta*)*alpha*-barrel architecture. Proteins 36(3):295-306.

Lynd LR, Zyl WHv, McBride JE, Laser M. 2005 Consolidated bioprocessing of cellulosic biomass: an update. Curr Opin Biotech:577.

Miller GL. 1959. Use of dinitrosalicylic acid reagent for determination of reducing sugar. Anal Chem 31(3):426.

Miroux B, Walker JE. 1996. Over-production of proteins in *Escherichia coli*: mutant hosts that allow synthesis of some membrane proteins and globular proteins at high levels. J Mol Biol 260(3):289-298.

Miyazaki K, Takenouchi M, Kondo H, Noro N, Suzuki M, Tsuda S. 2006. Thermal stabilization of *Bacillus subtilis* family-11 xylanase by directed evolution. J Biol Chem 281(15):10236-42.

Murphy C, Powlowski J, Wu M, Butler G, Tsang A. 2011. Curation of characterized glycoside hydrolases of fungal origin. Database 2011.

Paës G, O'Donohue MJ. 2006. Engineering increased thermostability in the thermostable GH-11 xylanase from *Thermobacillus xylanilyticus*. J Biotechnol 125(3):338-50.

Paice M, Zhang X. 2005. Enzymes find their niche. Pulp Pap Canada 106(6):17-20.

Ragauskas AJ, Poll KM, Cesternino AJ. 1994. Effects of xylanase pretreatment procedures on nonchlorine bleaching. Enzyme Microb Tech 16(6):492-495.

Reetz MT, Carballeira JD. 2007. Iterative saturation mutagenesis (ISM) for rapid directed evolution of functional enzymes. Nat Protoc 2(4):891-903.

Reetz MT, D Carballeira J, Vogel A. 2006. Iterative saturation mutagenesis on the basis of B factors as a strategy for increasing protein thermostability. Angew Chem-Int Edit 45(46):7745-7751.

Rogers TA, Bommarius AS. 2010. Utilizing simple biochemical measurements to predict lifetime output of biocatalysts in continuous isothermal processes. Chem Eng Sci 65(6):2118-2124.

Roncero MB, Torres AL, Colom JF, Vidal T. 2005. The effect of xylanase on lignocellulosic components during the bleaching of wood pulps. Bioresource Technol 96(1):21-30.

Ruller R, Deliberto L, Ferreira TL, Ward RJ. 2008. Thermostable variants of the recombinant xylanase A from *Bacillus subtilis* produced by directed evolution show reduced heat capacity changes. Proteins 70(4):1280-93.

Sambrook J, Russell DW. 2001. Molecular Cloning: A Laboratory Manual: Cold Spring Harbor Laboratory Press.

Schmidt A, Kratky C, Schlacher A, Schwab H, Steiner W. 1998. Structure of the xylanase from *Penicillium simplicissimum*. Protein Sci 7(10):2081-2088.

Schymkowitz J, Borg J, Stricher F, Nys R, Rousseau F, Serrano L. 2005. The FoldX web server: an online force field. Nucleic Acids Res 33(suppl 2):W382-W388.

Selvaraj S, Gromiha MM. 1998. Importance of long-range interactions in (α/β)8 barrel fold. J Protein Chem 17(7):691-697.

Shallom D, Shoham Y. 2003. Microbial hemicellulases. Curr Opin Microbiol 6(3):219-28.

Silva IR, Larsen DM, Jers C, Derkx P, Meyer AS, Mikkelsen JD. 2013. Enhancing RGI lyase thermostability by targeted single point mutations. Appl Microbiol Biotechnol 97(22):9727-35.

Somerville C, Bauer S, Brininstool G, Facette M, Hamann T, Milne J, Osborne E, Paredez A, Persson S, Raab T and others. 2004. Toward a systems approach to understanding plant cell walls. Science 306(5705):2206-2211.

Song L, Laguerre S, Dumon C, Bozonnet S, O'Donohue MJ. 2010. A high-throughput screening system for the evaluation of biomass-hydrolyzing glycoside hydrolases. Bioresource Technol 101(21):8237-8243.

Song L, Siguier B, Dumon C, Bozonnet S, O'Donohue M. 2012. Engineering better biomass-degrading ability into a GH11 xylanase using a directed evolution strategy. Biotechnology For Biofuels 5(1):3.

Stephens DE, Rumbold K, Permaul K, Prior BA, Singh S. 2007. Directed evolution of the thermostable xylanase from *Thermomyces lanuginosus*. J Biotechnol 127(3):348-354.

Stephens DE, Singh S, Permaul K. 2009. Error-prone PCR of a fungal xylanase for improvement of its alkaline and thermal stability. FEMS Microbiol Lett.

Tina KG, Bhadra R, Srinivasan N. 2007. PIC: Protein Interactions Calculator. Nucleic Acids Res 35(suppl 2):W473-W476.

Viikari L, Kantelinen A, Sundquist J, Linko M. 1994. Xylanases in bleaching: From an idea to the industry. FEMS Microbiol Rev 13(2-3):335-350.

Wang M, Si T, Zhao H. 2012. Biocatalyst development by directed evolution. Bioresource Technol 115(0):117-125.

Watanabe T. 1989. Structural studies on the covalent bonds between lignin and carbohydrate in lignin-carbohydrate complexes by selective oxidation of the lignin with 2,3-dichloro-5,6-dicyano-1,4-benzoquinone: Wood Research Institute, Kyoto University. http://hdl.handle.net/2433/53279.

Wen S, Tan T, Zhao H. 2012. Improving the thermostability of lipase Lip2 from *Yarrowia lipolytica*. J Biotechnol 164(2):248-253.

Wu Q, Soni P, Reetz MT. 2013. Laboratory evolution of enantiocomplementary *Candida antarctica* lipase B mutants with broad substrate scope. J Am Chem Soc 135(5):1872-1881.

Wyman CE. 2007. What is (and is not) vital to advancing cellulosic ethanol. Trends Biotechnol 25(4):153.

Xie H, Flint J, Vardakou M, Lakey JH, Lewis RJ, Gilbert HJ, Dumon C. 2006. Probing the structural basis for the difference in thermostability displayed by family 10 xylanases. J Mol Biol 360(1):157-67.

You C, Huang Q, Xue H, Xu Y, Lu H. 2010. Potential hydrophobic interaction between two cysteines in interior hydrophobic region improves thermostability of a family 11 xylanase from *Neocallimastix patriciarum*. Biotechnol Bioeng 105(5):861-870.

Zhang SB, Wu ZL. 2011. Identification of amino acid residues responsible for increased thermostability of feruloyl esterase A from *Aspergillus niger* using the PoPMuSiC algorithm. Bioresource Technol 102(2):2093-6.

Zhang Z-G, Yi Z-L, Pei X-Q, Wu Z-L. 2010. Improving the thermostability of *Geobacillus stearothermophilus* xylanase XT6 by directed evolution and site-directed mutagenesis. Bioresource Technol 101(23):9272.

Zimmermann W. 1991. Degradation of environmental pollutants by microorganisms and their metalloenzymes. In: Sigel H, Sigel A, editors. Bacterial Degradation of Hemicelluloses. New York Marcel Dekker. p 357–398.

Figure Caption

Figure 1. Representative example of screening results of randomly mutagenized Xyn10A library. Results of recombinants from one microplate are shown here. The 96-well microplate was heat-treated for 15 min at 58°C. The residual activity of each library individual is indicated by grey bars and for the three wild-type controls by white bars (far right of the figure).

Figure 2. Evaluation of Xyn10A thermostability by (A) $t_{1/2}$ 60°C and (B) T_m. The letters A, B, C and D correspond to saturation mutagenesis randomized at position 25, 29/31, 43 and 58, respectively.

Figure 3. Thermoactivity of -wild-type and thermostable mutants of Xyn10A.

Figure 4. (A) Tertiary structure of variant 4S1 Swiss-model and localization of beneficial residues Ala-29, Leu-31, Phe-43 and Ile-58 at N-terminal coil, helix α0, strand β1 and helix α1, respectively. (B) Schematic diagrams of residues involved in putative hydrophobic interactions with Leu-31, Phe-43 and Ile-58.

Figure 5. (A) Partial alignment of the N-terminal sequences of –wild-type Xyn10A, variant 4S1 and other fungal thermostable GH10 xylanases. With the exception of wild-type and 4S1 Xyn10A, the other xylanases are named according to their microbial origin, and all proteins are labeled with their optimal temperatures. All sequences and temperature optima information were obtained from *myco*CLAP database (https://mycoclap.fungalgenomics.ca) (Murphy et al. 2011) and signal peptides were deleted. The selected thermostable xylanases are from *Chrysosporium lucknowense* (CLX1 and CLX3), *Thermoascus aurantiacus* (TAX), *Aureobasidium pullulans* (APX), *Penicillum simplicissinum* (PSX), *Aspergillus terreus* (ATX) and *Aspergillus oryzae* (AOX). (B) Partial alignment of the N- and C-terminal sequences of 4S1 and three bacterial GH10 xylanases from *Bacillus halodurans* S7 (BHX), *Bacillus firmus* (BFX) and *Bacillus sp.* NG-27 (BSX). Sequences of three *Bacillus* xylanases were obtained from database of Protein Data Bank. In both A and B panels, the five mutational amino acids in 4S1 and their equivalent residues in other xylanases are shaded in black.

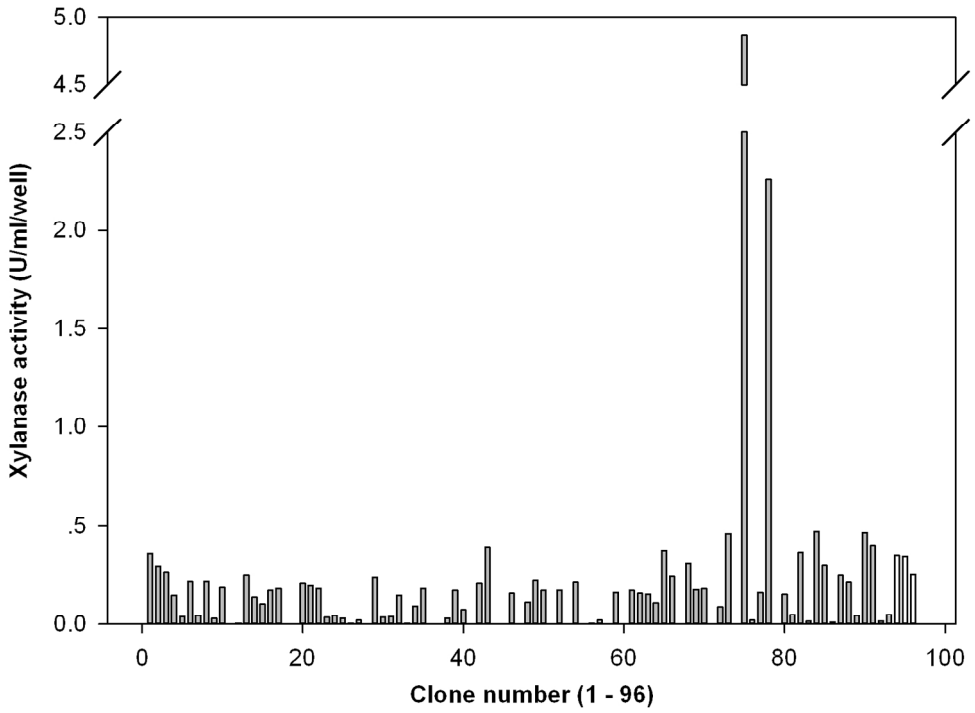

Representative example of screening results of randomly mutagenized Xyn10A library. Results of recombinants from one microplate are shown here. The 96-well microplate was heat-treated for 15 min at 58°C. The residual activity of each library individual is indicated by grey bars and for the three wild-type controls by white bars (far right of the figure).
147x115mm (300 x 300 DPI)

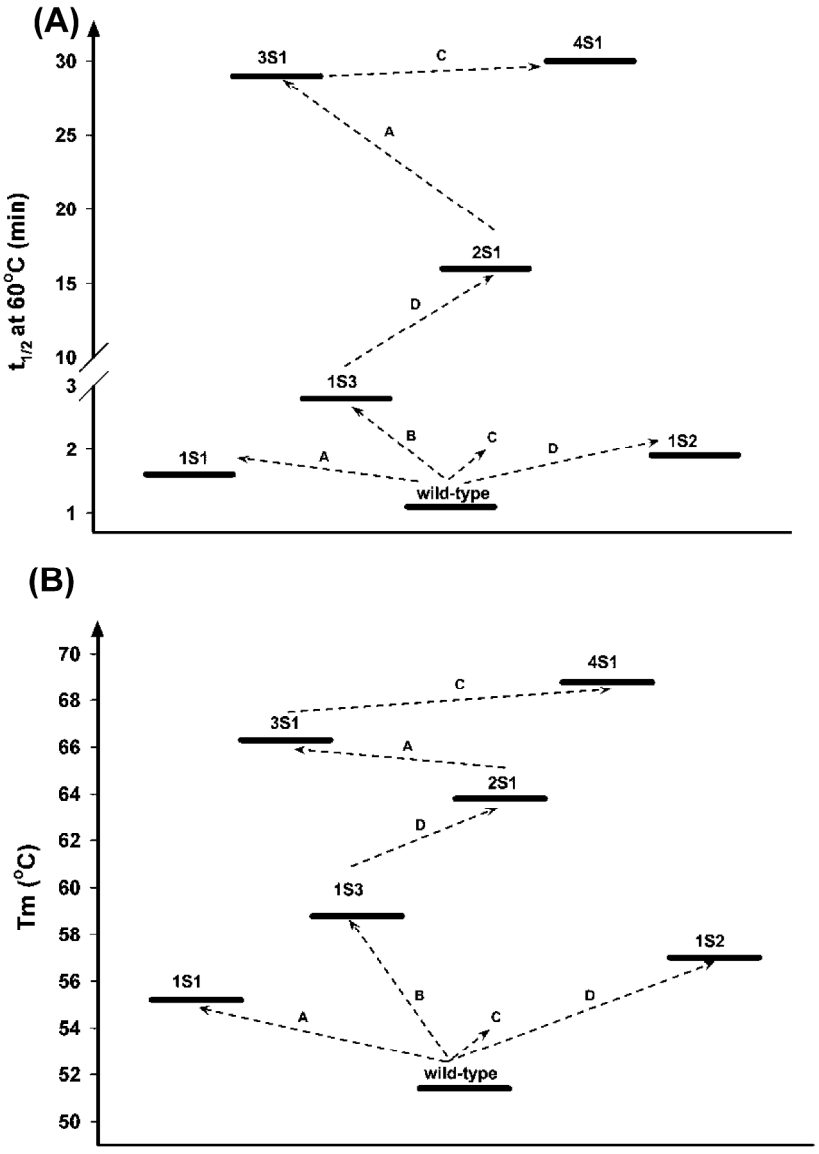

Figure 2. Evaluation of Xyn10A thermostability by (A) *t1/2* 60°C and (B) *Tm*. The letters A, B, C and D correspond to saturation mutagenesis randomized at position 25, 29/31, 43 and 58, respectively.
239x337mm (600 x 600 DPI)

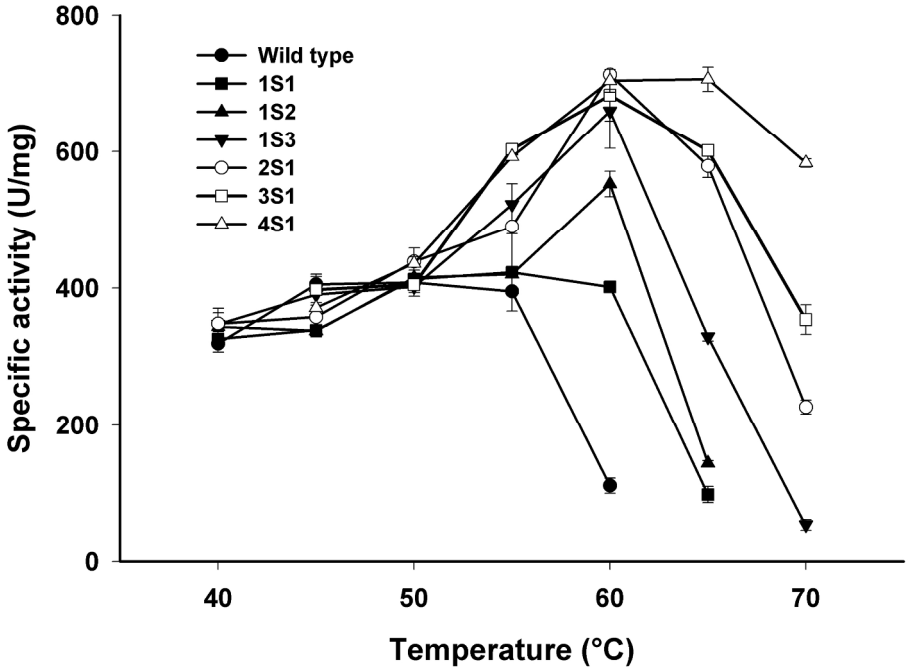

Figure 3. Thermoactivity of wild-type and thermostable mutants of Xyn10A.
124x95mm (600 x 600 DPI)

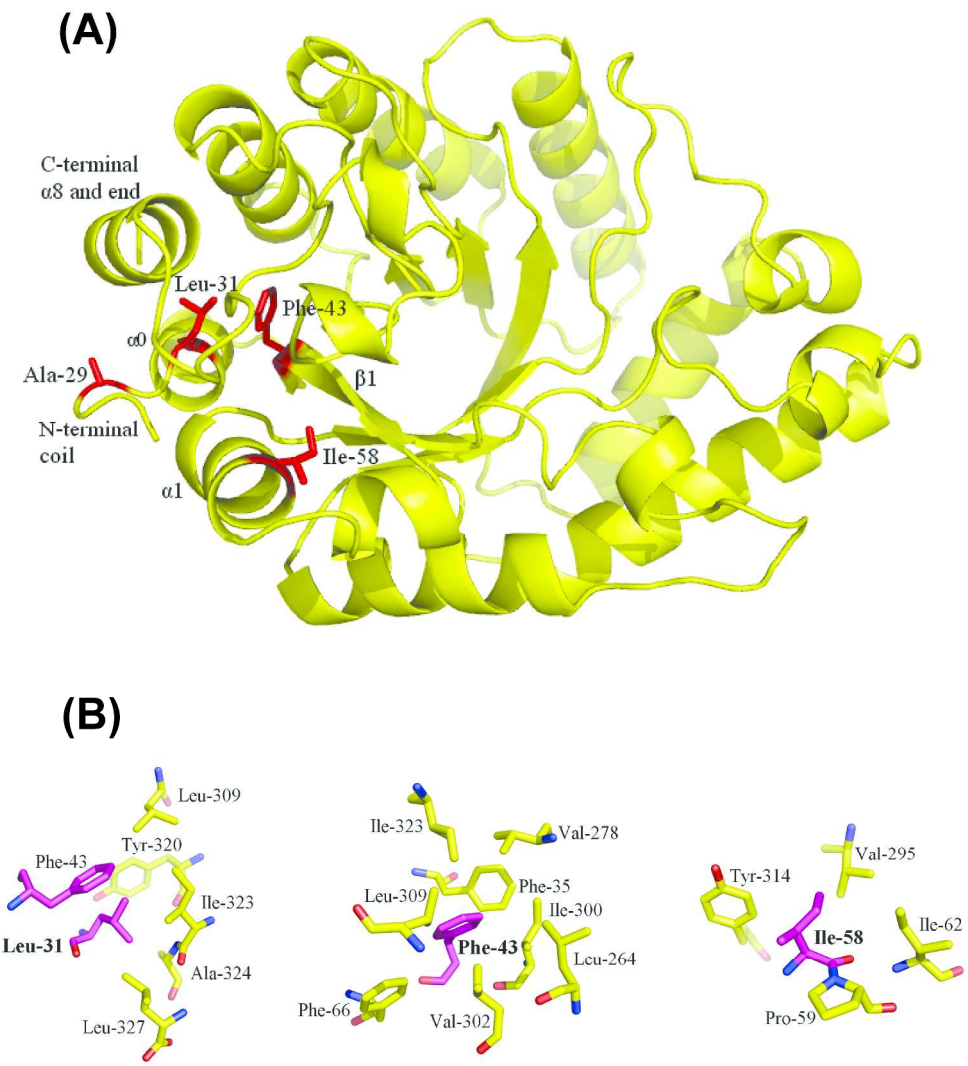

Figure 4. (A) Tertiary structure of variant 4S1 Swiss-model and localization of beneficial residues Ala-29, Leu-31, Phe-43 and Ile-58 at N-terminal coil, helix α0, strand β1 and helix α1, respectively. (B) Schematic diagrams of residues involved in putative hydrophobic interactions with Leu-31, Phe-43 and Ile-58.
206x219mm (600 x 600 DPI)

Figure 5. (A) Partial alignment of the N-terminal sequences of wild-type Xyn10A, variant 4S1 and other fungal thermostable GH10 xylanases. With the exception of wild-type and 4S1 Xyn10A, the other xylanases are named according to their microbial origin, and all proteins are labeled with their optimal temperature. All sequences and temperature optima information were obtained from *mycoCLAP* database (https://mycoclap.fungalgenomics.ca) (Murphy et al. 2011) and signal peptides were deleted. The selected thermostable xylanases are from *Chrysosporium lucknowense* (CLX1 and CLX3), *Thermoascus aurartiacus* (TAX), *Aureobasidium pullulans* (APX), *Penicillum simplicissium* (PSX), *Aspergillus terreus* (ATX) and *Aspergillus oryzae* (AOX). (B) Partial alignment of the N- and C-terminal sequences of 4S1 and three bacterial GH10 xylanases from *Bacillus halodurans* S7 (BHX), *Bacillus firmus* (BFX) and *Bacillus* sp. NG-27 (BSX). Sequences of three *Bacillus* xylanases were obtained from database of Protein Data Bank. In both A and B panels, the five mutational amino acids in 4S1 and their equivalent residues in other xylanases are shaded in black.
119x57mm (600 x 600 DPI)

Table 1. Oligonucleotide primer pairs applied in site-saturation mutagenesis.

Randomized position	Annealing temperature (°C)	Primer sequence[1] (5'→ 3')
25	70	CATTGAACCC**NNK**CAGGCTTCAG GGCTCCATATGTATATCTCCTTCTTAAAGTTAAAC
29 and 31	72	CCGTCAGGCTTCA**NNK**AGT**NNK**GATACCAAATTCAAG GGTTCAATGGGCTCCATATGTATATCTCCTTCTTAAAGTTAAAC
43	67	GGAAGAAATAT**NNK**GGAAACATTGG CGTGAGCCTTGAATTTGGTATC
58	72	CCAAGAACTCGAAG**NNK**CCGGCCATTATCAAG TCAAGGTGTACTGATCACCAATGTTTCCAAG

[1] Randomized positions are highlighted in boldface with an underline. N = G, A, T or C; K = G or T.

Table 2. Thermoresistance of Xyn10A mutants from a random mutagenesis library

Selected frequency	Enzymes	Codon change[1]	Amino acid substitution[2]	% Residual activity[3]		
				58°C, 15min	60°C, 10min	65°C, 5min
	wild-type	—	—	0.8±0.1%	0.2±0.1%	0.0%
1	R1H01	G20T/C73T	R25C/L43F	10.8±1.7%	4.5±1.2%	2.0±0.9%
1	R1H02	C19T/C119T/C137T	R25C/T58I/A64V	8.8±1.8%	2.2±0.3%	1.0±0.5%
4	R1H03	T32A	V29E	4.8±0.5%	0.6±0.2%	0.2±0.1%
1	R1H04	A30T/T32A				
1	R1H05	T32C	V29A	2.1±0.4%	0.6±0.4%	0.3±0.2%
1	R1H06	G31C	V29L	15.0±1.1%	11.6±1.7%	1.2±0.7%
1	R1H07	G31T				
1	R1H08	G31C/A36C/T90C	V29L/I31L	20.1±4.7%	10.0±2.1%	3.4±1.3%
1	R1H09	G31T/G194T	V29L/S83I	4.5±1.0%	2.2±0.3%	0.2±0.0%
1	R1H10	A34G	S30G	2.6±0.2%	1.2±0.1%	0.3±0.0%
1	R1H11	A43G/C147T	T33A	4.6±1.0%	1.7±0.8%	0.0%
2	R1H12	A47G	K34R	3.5±1.0%	1.1±0.8%	0.0%
1	R1H13	A47G/C192T				
1	R1H14	C45T/A46C	K34Q	6.6±0.9%	2.6±2.0%	0.0%
2	R1H15	A46G	K34E	2.1±0.6%	0.9±0.0%	0.2±0.0%
1	R1H16	C73T	L43F	4.9±0.4%	2.2±0.5%	0.5±0.1%
1	R1H17	C119T/C165T	T58I	20.7±2.1%	8.8±6.0%	3.1±2.2%
2	R1H18	C119T				
1	R1H19	C60A/C119T	H38Q/T58I	1.2±0.3%	0.8±0.4%	0.0%
1	R1H20	A245T	Q100L	2.3±0.2%	0.1±0.1%	0.0%
1	R1H21	T94A/A219T/A245T	Y50N/Q100L	2.4±1.0%	1.1±0.3%	0.0%

[1] nucleotide numbering is based on the cloned DNA insert in pET-20b.

[2] amino acid numbering is based on pre-Xyn10A protein sequence

[3] Results based on 8 biological replicates (±sd)

Table 3. Thermostability data of top Xyn10A mutants selected from ISM libraries

Iteration	Template	Saturated site	Best hit variant	Amino acid substitutions	% Residual activity			60°C $t_{1/2}$ min	T_m °C
					60°C, 20 min	65°C, 10 min	70°C, 6 min		
1st	wild-type	25	1S1	R25W	0.5±0.1%[1]	0.2±0.0%[1]	< 0.1%[1]	1.6[2]	55.2
		29 and 31	1S2	V29A-I31L	9.2±2.3%[1]	0.4±0.1%[1]		1.9[2]	57.0
		43	N/A						
		58	1S3	T58I	3.0±0.8%[1]	0.2±0.1%[1]	< 0.1%[1]	2.8[2]	58.8
2nd	1S2	58	2S1	V29A/I31L/T58I	40.6±1.4%[2]	15.3±2.1%[2]	-	16.0[2]	63.8
3rd	2S1	25	3S1	R25W/V29A/ I31L/T58I	60.4±2.8%[2]	37.3±2.2%[2]	5.5±1.3%[2]	29.0[2]	66.3
4th	3S1	43	4S1	R25W/V29A/I31L/L43F/T58I	64.1±0.5%[2]	37.1±1.3%[2]	8.0±1.9%[2]	30.0[2]	68.8

[1] Values obtained with cell extracts using the high-throughput assay described in the Materials and Methods section and results based on 8 biological replicates (±sd)

[2] Values obtained with purified enzyme preparations using the thermal inactivation assay described in the Materials and Methods section.

Table 4. Steady-state kinetics[1] of wild-type and two top thermostable mutants of Xyn10A

Michaelis–Menten parameters[1]	Temperature	Enzymes		
		Wild-type	3S1	4S1
	50°C			
k_{cat} (s^{-1})		32.7±1.2	36.4±1.5	33.4±0.8
$K_{m\ app}$ (g l^{-1})		6.2±0.5	7.1±0.6	6.6±0.5
$k_{cat}/K_{m\ app}$ (l s^{-1} g^{-1})		5.31	5.10	5.09
	60°C			
k_{cat} (s^{-1})		-	53.5±2.3	51.1±2.3
$K_{m\ app}$ (g l^{-1})		-	7.0±0.7	6.6±0.6
$k_{cat}/K_{m\ app}$ (l s^{-1} g^{-1})		-	7.67	7.69

[1] Steady state kinetics were determined as described in Materials and Methods using beechwood xylan as substrate